Chinese Journal of
POLYMER SCIENCE

RESEARCH ARTICLE

https://doi.org/10.1007/s10118-023-2974-7
Chinese J. Polym. Sci. **2023**, *41*, 1425–1438

Molecular Dynamics Simulations of Stretch-Induced Crystal Changes in Crystallized Polyethylene/Carbon Nanotubes Nanocomposites

Yu-Hang Zhou, Jun Yang, Zhi-Ping Zhou, Tong-Fan Hao, and Yi-Jing Nie*

Research School of Polymeric Materials, School of Materials Science and Engineering, Jiangsu University, Zhenjiang 212013, China

Electronic Supplementary Information

Abstract Understanding deformation mechanisms in semi-crystalline polymers during stretching is useful for guiding the processing of high-performance polymer products. In the current work, molecular dynamics simulations were performed to investigate the crystal changes in crystallized polyethylene/carbon nanotube nanocomposites during uniaxial stretching. Both crystal fragmentation and melting occur at low strains. Crystals with small sizes are easier to melt, while those with large sizes would break into smaller crystals. In addition, crystals in interfacial regions are more likely to melt or break due to the orientation motion of carbon nanotubes. It was also found that the recrystallization process is closely related to the stretch-induced orientation of chain segments. After orientation of chain segments along stretching direction is saturated, the recrystallization of highly oriented segments dominates. The current simulation findings are effective complements to the theories of the mechanism of plastic deformation in semicrystalline polymers.

Keywords Molecular dynamics simulation; Carbon nanotubes; Stretching; Melting and recrystallization

Citation: Zhou, Y. H.; Yang, J.; Zhou, Z. P.; Hao, T. F.; Nie, Y. J. Molecular dynamics simulations of stretch-induced crystal changes in crystallized polyethylene/carbon nanotubes nanocomposites. *Chinese J. Polym. Sci.* **2023**, *41*, 1425–1438.

INTRODUCTION

With the rapid developments of industry in modern society, more demands are put forward for the mechanical properties of composite materials. In addition, the development concept of low carbon and low energy consumption is gaining popularity. Polymer nanocomposites can precisely meet the requirements of high mechanical properties, low carbon and low energy consumption. The mechanical properties of polymeric materials, such as modulus and tensile strength, can be greatly improved by filling a small number of nanoparticles into polymer matrix.[1–5] Compared with traditional polymer composites, polymer nanocomposites have higher mechanical strength and lower density, which helps to reduce energy consumption.

For semi-crystalline polymers, the addition of nanoparticles can influence their crystallization behaviors, so as to further affect the mechanical properties. For instance, it was reported that the crystallization rate of semi-crystalline polymers can be effectively accelerated and the crystalline morphologies can be changed due to the introduction of carbon nanotubes (CNTs),[6–13] and the corresponding mechanical properties are thus significantly improved.[1,3,4] Besides, the presence of nanoparticles can also affect the microstructural changes of semi-crystalline polymers during stretching.[2,4,14–17]

For polyolefin materials, complex crystal structure changes occur in the process of stretching, including slip, rotation/orientation, fragmentation, melting and recrystallization of lamellar crystals.[18–29] Since nanoparticles can affect the orientations of chain segments and limit the conformations and movements of chains,[1,2,4,6–13,15,16] they will inevitably influence the motions, fragmentation, melting-recrystallization and other processes of crystals during stretching, thus affecting the mechanical properties of polymer materials. Though many research results have been obtained in the study of the structural evolutions of semi-crystalline polymers during drawing process,[17–29] there are few studies focusing on the effects of nanoparticles on the stretch-induced structural evolutions of polyolefin nanocomposites.[17]

In addition to the advanced experimental methods, such as *in situ* synchrotron small-angle X-ray scattering and wide-angle X-ray diffraction experiments,[17,30–35] several groups also used molecular simulations to probe polymer crystallization,[8,26,27,36–54] including the changes of polymer crystals during plastic deformation.[55–60] For instance, Yamamoto applied molecular dynamics (MD) simulations to investigate the stretch-induced structure changes in the crystallized PE systems along the fiber axis and along the transverse direction.[58] It was found that the stretching along the fiber axis causes reorientation of the tilted chains and chain slips in the crystals, but the transverse stretching leads to the melting and recrystallization of oriented crystals.[58] Rutledge *et al*.

* Corresponding author, E-mail: nieyijing@ujs.edu.cn

Special Issue: Theory and Simulation of Macromolecules
Received February 6, 2023; Accepted February 28, 2023; Published online April 18, 2023

focused on the effects of strain rate and temperature.[57] They observed that the cavitation in non-crystalline domains dominates the structural changes if the crystallized PE system was stretched at a high temperature with a fast strain rate, while repeated melting/recrystallization events occur if the system was stretched at a high temperature with a slow strain rate.[57] Using dynamic Monte Carlo simulations, Hu and coworkers also detected that the melting-recrystallization process takes place in the crystals during stretching.[37]

In the current simulations, we use MD simulations to probe the stretch-induced structural evolutions in the crystallized PE/CNT nanocomposites, and found that the existence of CNTs has significant effects on the crystal melting process during stretching. Those simulation findings can provide some theoretical supports for the preparation of high-performance polyolefin/CNT nanocomposites.

SIMULATION DETAILS

The initial states of the corresponding polyethylene (PE)/CNT nanocomposite systems were built using the EMC software (version 9.4.4).[61] Four PE/CNT nanocomposite systems were constructed to investigate the influences of the length and the content of CNTs on the stretch-induced melting-recrystallization process of PE. 200 PE chains and several CNTs were placed into the cubic simulation box, the side length of which was 212.96 Å. Periodic boundary conditions were adopted in *X*-, *Y*- and *Z*-axis directions. The united-atom (UA) model was used to simulate PE chains, and then each PE chain contains 200 UA units. Compared with the all-atom model, the simulations using the UA model exhibit much higher simulation efficiency. Besides, the dynamic behaviors (*e.g.*, the crystallization behaviors) in the corresponding stretched systems could be effectively reflected on the basis of the all-atom model.[49] Thus, we used the all-atom model in the current simulation work. CNTs (armchair (7, 7) with different lengths (36.89 and 73.78 Å) and different contents (3.5 wt% and 6.7 wt%)) were introduced, as listed in Table 1. Fig. 1 illustrates the initial model of the PE/CNT nanocomposite system with the CNT length of 73.78 Å and the CNT content of 6.7 wt% (namely, the L73-4 system). After the modeling process was completed, the subsequent simulations were performed using the LAMMPS package.[62]

The force field of Paul *et al*. was applied for the intermolecular and intramolecular interactions between the UA units of PE chains,[63] as shown in Table S1 in the electronic supplementary information (ESI). Besides, the AIREBO potential function was used to simulate the interactions between the CNTs,[64] and the L-J potential function was used for the interfacial interactions between the PE chain segments and the CNTs (the values of the corresponding parameters can also be seen in Table S1 in ESI).

The specific simulation process is shown in Fig. 2. Firstly, the relaxation process was performed based on the NPT ensemble to achieve equilibrium state at T = 600 K, with a duration of 10 ns and the timestep of 1 fs. The Rouse relaxation time of PE chains in the current simulations at T = 600 K is 5.78 ns, which is shorter than the simulation time for relaxation (10 ns). Thus, the equilibrium state of the PE chains could be obtained. Secondly, the isothermal crystallization process (the NPT ensemble) was performed at T = 400 K, with a duration of 30 ns and the timestep of 1 fs. Finally, with the temperature unchanged (the NVT ensemble), the crystallized system was stretched along the *X*-axis direction at a strain rate of 10^{10} s^{-1} to the strain of 6. The Verlet algorithm was used to integrate the motion equation during simulations.

Table 1 The established PE/CNT nanocomposite systems in simulations.

Length (Å)	Number	Mass fraction (wt%)	Abbreviation
36.89	4	3.5	L36-4
	8	6.7	L36-8
73.78	2	3.5	L73-2
	4	6.7	L73-4

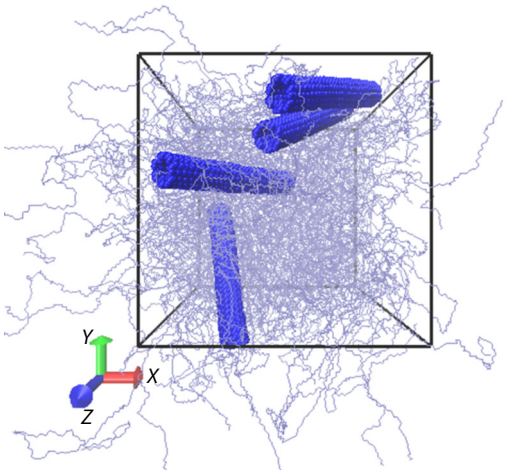

Fig. 1 Snapshot of the initial model of the L73-4 system.

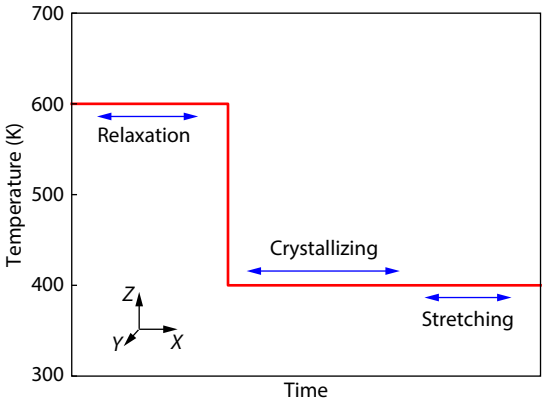

Fig. 2 Diagram of simulation process containing three different parts: relaxation process, isothermal crystallization process and stretching process.

RESULTS AND DISCUSSION

Quiescent Crystallization of PE/CNT Nanocomposites

Fig. 3(a) shows the variations of the crystallinity of the four PE/CNT nanocomposite systems (XC1) during the quiescent crystallization process. The definition of crystallinity is shown in ESI. The crystallinity of the four PE/CNT nanocomposite systems increases with the increase of simulation time, indicating that isothermal crystallization occurs in the four systems. In order to reveal the effects of the CNTs on PE crystallization, the

https://doi.org/10.1007/s10118-023-2974-7

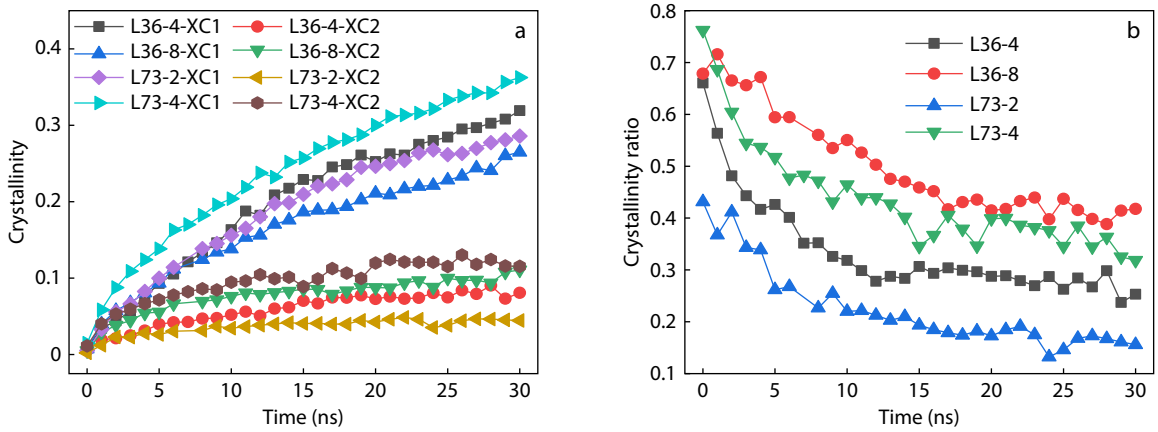

Fig. 3 (a) Variations of polymer crystallinity of the PE/CNT nanocomposite systems and the interfacial regions; (b) The ratio of polymer crystallinity of the interfacial regions to the total crystallinity of the PE/CNT nanocomposite systems.

crystallinity of the chain segments in the interfacial regions of the four systems (XC2) was also calculated, as also shown in Fig. 3(a). The interfacial regions were defined as the regions within 3 times the radius of the CNTs from the surfaces (about 1.424 nm). It can also be seen that the crystallinity of the interfacial regions also increases with the increase of simulation time, which is lower than the corresponding crystallinity of the whole systems (the volume of the interfacial regions is obviously smaller than that of the whole systems), implying that polymer crystallization also takes place in the interfacial regions.

In order to observe polymer crystallization in the interfacial regions more clearly, the ratio of the polymer crystallinity of the interfacial regions to the crystallinity of the whole systems was counted, as shown in Fig. 3(b). It can be observed that the crystallinity ratio at the initial stage of crystallization is highest, and then gradually decreases as the crystallization process progresses. These results suggest that the initial positions of PE crystal nuclei are mainly in the interfacial regions, and the heterogeneous nucleation of PE chain segments on the CNT surfaces is dominant. Some PE chain segments would be adsorbed around the CNTs under the influence of the interfacial interactions between the PE chain segments and the CNTs. In the process of quiescent crystallization, those adsorbed chain segments have relatively lower free energy barrier for heterogeneous nucleation due to the lower surface energy of crystal nuclei nucleated on the CNT surfaces,[1,4,8,10,65] which makes those adsorbed segments have stronger heterogeneous nucleation ability than the other chain segments away from the CNT based on homogeneous nucleation mode. As the polymer crystallization continues, on one hand, the crystals based on heterogeneous nucleation grow up gradually, and then chain segments outside the interfacial regions can also participate in the growth process of those crystals; on the other hand, chain segments away from the CNTs can also form crystal nuclei through homogeneous nucleation mode. In short, more crystals grow up in the non-interfacial regions, resulting in the decrease of the ratio of the crystallinity of the interfacial regions to that of the whole systems. In addition, it can also be seen in Fig. 3(b) that under the same simulation times, the crystallinity ratio in the PE/CNT nanocomposite systems with the high CNT contents (the L36-8 and the L73-4 systems) is higher than that in the systems with the low CNT contents (the L36-4 and the L73-2 systems), indicating that more chain segments in the systems with the higher CNT contents are involved in the crystallization based on the heterogeneous nucleation mode, attributed to the presence of more interfacial regions.

For the crystallization process of PE, the corresponding crystal nuclei are formed by the aggregation of local segments with trans-conformations.[35,47,66] Therefore, in order to display the heterogeneous nucleation process of the chain segments in the interfacial regions induced by the CNTs, the spatial distributions of the aggregation regions of local segments with trans-conformations in the four different systems at the crystallization time of 0.13 ns were further drawn, as shown in Fig. 4. The definition of the aggregation regions of local segments with trans-conformations can be seen in ESI.[66] It can be seen that the aggregation regions of local segments with trans-conformations appear in the interfacial regions at the early stage of crystallization, which then develop into crystallites, demonstrating that the CNTs have the ability to induce the heterogeneous nucleation of PE chain segments in the interfacial regions.[1,4,6–8,10,67,68]

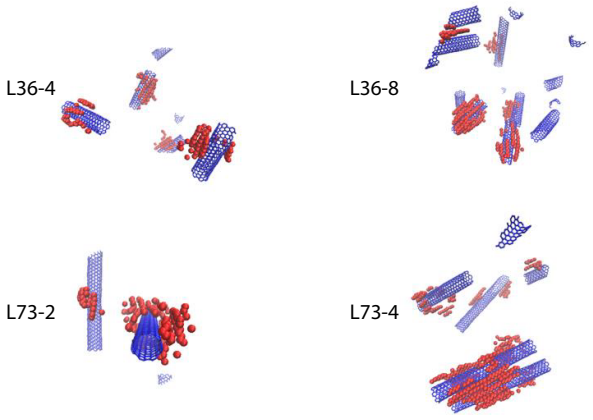

Fig. 4 Snapshots of aggregation regions of local segments with trans-conformations in the four systems at the crystallization time of 0.13 ns; the red spheres are the segments belonging to the aggregation regions of local segments with trans-conformations, and the CNTs are drawn with blue color.

https://doi.org/10.1007/s10118-023-2974-7

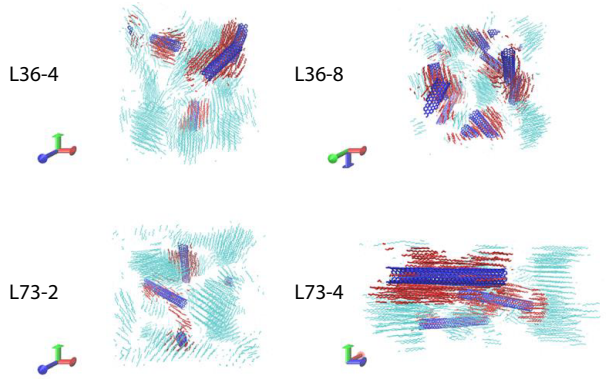

Fig. 5 Snapshots of final crystal morphologies in the four systems formed at the crystallization time of 30 ns; the red lines denote the crystalline stems in the interfacial regions, and the green lines denote the crystalline stems in the non-interfacial regions. The red arrows represent the *X*-axis direction, the green arrows represent the *Y*-axis direction, and the blue arrows represent the *Z*-axis direction.

Fig. 5 shows the snapshots of the crystalline morphologies of the four systems at the later stage of crystallization (the crystallization time of 30 ns). Only crystalline bonds were shown in Fig. 5 (the definition of crystalline bonds can be seen in the Supporting Information). As shown in Fig. 5, there are more crystals based on homogeneous nucleation mode in the L36-4 system and the L73-2 system due to the small amount of the CNTs (the red lines in Fig. 5). However, in the L36-8 and the L73-4 systems, more crystals based on the heterogeneous nucleation of chain segments induced by the CNTs appear, due to the presence of more CNTs. In addition, the crystalline stems in the interfacial regions exhibit the same orientation as the long axis of the corresponding center CNTs, which is consistent with the previous experimental and simulation results.[1,3,4,6,8,10–13,41]

In order to further elucidate the microscopic mechanism of the heterogeneous nucleation of PE chain segments induced by the CNTs, the effects of the CNTs on the orientations of chain segments were investigated. Fig. 6(a) shows the orientational-order parameters (*P*) of the long axis of the CNTs along the *X*-axis direction. The orientational-order parameters of PE bonds and CNT axes along the corresponding directions were calculated on the basis of this following equation:

$$P = \left\langle \frac{3\cos^2(\phi_i) - 1}{2} \right\rangle = \frac{3}{2}\left\langle (\vec{e}_i.\vec{e}_x)^2 \right\rangle - \frac{1}{2} \quad (1)$$

where $\vec{e}_i$ is the bond vector in PE chains located at the i^{th} bead (regarded as the vector from bead i–1 to bead i+1) or the axial vector of the i^{th} CNT, $\vec{e}_x$ is the vector along the stretching direction or the CNT axes, ϕ_i is the angle between $\vec{e}_i$ and $\vec{e}_x$, and ⟨⟩ indicates the statistical average of the corresponding

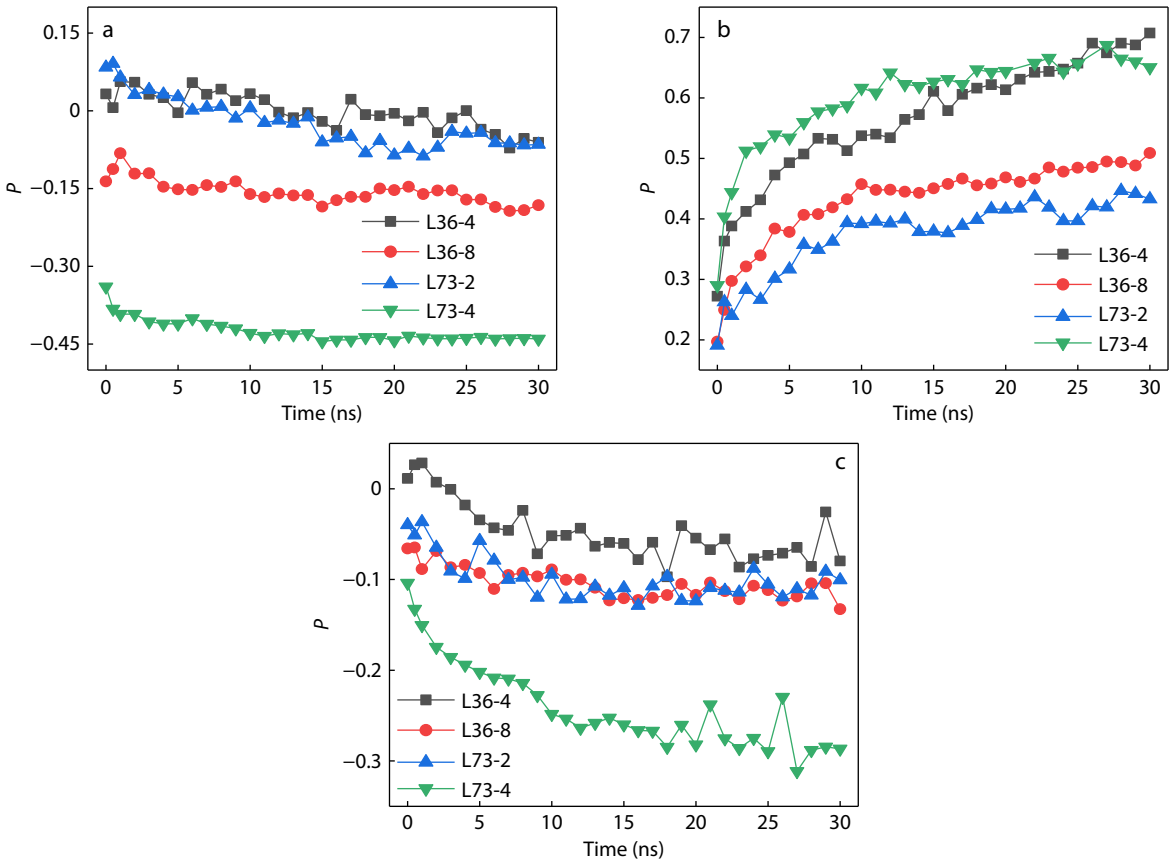

Fig. 6 (a) Orientational-order parameters of the CNT axes in the four systems along the *X*-axis during quiescent crystallization; (b) Orientational-order parameters of PE bonds in interfacial regions in the four systems along the CNT axes during quiescent crystallization; (c) Orientational-order parameters of PE bonds in interfacial regions in the four systems along the *X*-axis during quiescent crystallization.

https://doi.org/10.1007/s10118-023-2974-7

calculated values for the PE bonds or the CNT axes. The value of *P* can be used to reflect the degree of orientation of the PE bonds or the CNT axes. It can be seen that the orientational-order parameters of the long axis of the CNTs along the *X*-axis direction are nearly unchanged, suggesting that there is no obvious orientation process of the CNTs in each system along the *X*-axis direction during the quiescent crystallization. It can also be seen that the orientational-order parameters of the long axis of the CNTs along the *X*-axis direction in the L73-4 system are lowest (in the range of −0.445 to −0.339). Combined with the results in Fig. 5, it can be demonstrated that the long axes of the CNTs in the L73-4 system are perpendicular to the *X*-axis direction. The orientational-order parameters of the long axes of the CNTs in the L36-4 and the L73-2 systems are close to 0, indicating that the CNTs in those two systems exhibit random orientations with respect to the *X*-axis direction. Figs. 6(b) and 6(c) show the orientational-order parameters of PE bonds in the interfacial regions along the long axis of the corresponding center CNTs and along the *X*-axis direction in the four systems, respectively. It can be observed that the orientational-order parameters of the PE bonds along the long axis of the CNTs gradually increase with the progress of crystallization. This indicates that the orientation of the PE bonds in the interfacial regions is closely related to that of the long axes of the CNTs during crystallization. Our previous simulation work demonstrated that the one-dimensional nanofillers can induce interfacial chain segments to orient along their long axes and then form oriented crystallites on the basis of heterogenous nucleation.[8–13,41] However, the orientational-order parameters of the PE bonds in the interfacial regions along the *X*-axis direction decrease, because the corresponding chain segments are affected by their adjacent CNTs and will orient along the long axes of the adjacent CNTs.

Structural Changes during Stretching

Subsequently, we studied the microstructure changes of the crystallized PE/CNT nanocomposite systems during stretching. Fig. 7(a) shows the changes of the polymer crystallinity of the whole systems during stretching. It can be seen that the polymer crystallinity of the whole systems decreases and then increases after a minimum crystallinity value during stretching, indicating that the crystals formed in the quiescent crystallization melt due to stretching, and then amorphous chain segments recrystallize at high strains. The stretch-induced melting and recrystallization processes have been observed in the stretching of crystallized semi-crystalline polymers in many experiments.[17,19,23,25,28,29,32] Similar stretch-induced melting and recrystallization phenomena were also reported in the simulation work of Yamamoto[58] and Rutledge *et al.*[55–57] In order to see more clearly the difference in the variations of polymer crystallinity in the different systems, the differences

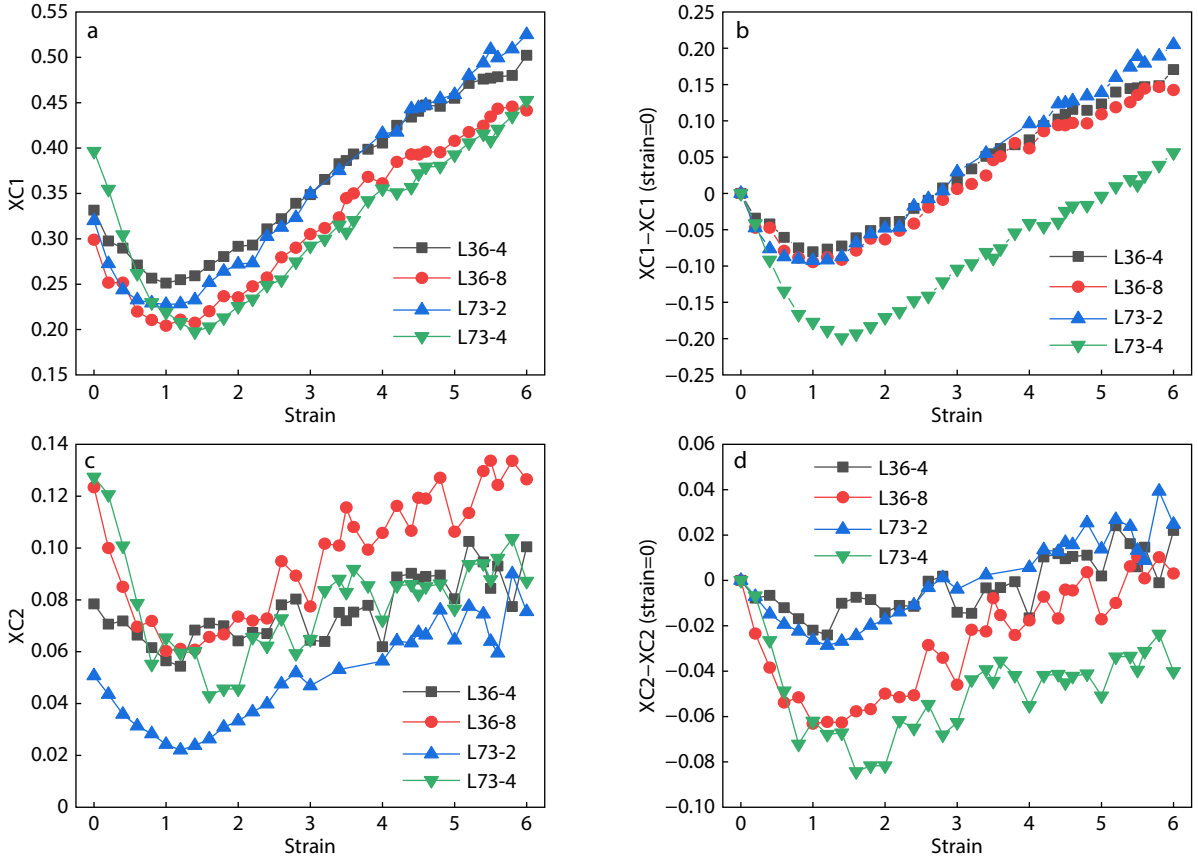

Fig. 7 (a) Changes of polymer crystallinity of the whole systems during stretching; (b) Changes of the differences between the crystallinity of the whole systems and the corresponding crystallinity at the strain of 0 during stretching; (c) Changes of polymer crystallinity of the interfacial regions during stretching; (d) Changes of the differences between the crystallinity of the interfacial regions and the corresponding crystallinity at the strain of 0 during stretching.

https://doi.org/10.1007/s10118-023-2974-7

between the crystallinity and the corresponding crystallinity at the strain of 0 (XC1-XC1(strain = 0)) were further calculated, as shown in Fig. 7(b). It can be seen that the minimum values of the crystallinity differences in the L36-8 system and the L73-4 system are lower than that in the L36-4 system and the L73-2 system, respectively, indicating that more crystals melt at low strains during stretching in the systems filled with more nanofillers. In addition, it can also be seen in Fig. 7(b) the minimum values of the crystallinity differences in the L73-2 system and the L73-4 system are lower than that in the L36-4 system and the L36-8 system, respectively, implying that more crystals melt in the systems containing longer CNTs due to stretching.

Then, we further calculated the crystallinity variations in the interfacial regions during stretching, as shown in Fig. 7(c). It can be seen that the crystallinity of the interfacial regions also decreases at first and then increases during stretching, similar to the crystallinity of the whole systems. In other words, stretching can cause the melting of the crystals and the recrystallization of amorphous chain segments in the interfacial regions. As shown in Fig. 7(d), it can be observed that the systems with the higher CNT contents (the L36-8 system and the L73-4 system) exhibit the lower minimum values of the crystallinity differences compared with those with the lower CNT contents (the L36-4 system and the L73-2 system), respectively, and the systems with the longer CNTs (the L73-2 system and the L73-4 system) exhibit the lower minimum values of the crystallinity differences compared with those with the short CNTs (the L36-4 system and the L36-8 system), respectively. This means that the presence of the CNTs can significantly affect the stretch-induced crystal melting. In the systems with the higher CNT contents, there are more crystals in the interfacial regions (as seen in Fig. 3b). Those crystals in the interfacial regions would be affected by the motions of the CNTs during stretching, resulting in the melting of more crystals. In order to confirm that the crystals in the interfacial regions are easier to melt during stretching, the ratios of the maximum value of crystallinity decrease in the whole systems/in the interfacial regions to the corresponding initial crystallinity values at the state before stretching (strain = 0) were calculated, respectively, as shown in Fig. 8(a). The ratio of the values of crystallinity decrease in the interfacial regions is apparently higher than that in the whole systems, demonstrating that the crystals in the interfacial regions are more susceptible to the stretching. Fig. 8(b) shows the average crystallization rates at the two stretching stages (the stretch-induced crystal melting stage and the stretch-induced polymer recrystallization stage) in the whole systems and in the interfacial regions, respectively. In Fig. 8(b), the data greater than zero correspond to the crystallization rates in the stretch-induced polymer recrystallization stage, and the data less than zero correspond to the crystallization rates in the stretch-induced crystal melting stage. The crystallization rates were obtained by the linear fitting of the crystallinity curves in the two different stages of the corresponding systems. It can be observed in Fig. 8(b) that there are no obvious differences in the crystallization rates in the stretch-induced polymer recrystallization stage of the four systems, indicating that the recrystallization process was not significantly affected by the CNT content or length. However, it can also be seen that the crystallization rate in the stretch-induced crystal melting stage of the L36-8 system is slightly lower than that of the L36-4 system and the L73-2 system, and the crystallization rate in the stretch-induced crystal melting stage of the L73-4 system is the lowest, indicating that the crystals melt faster during stretching in the systems with the higher CNT contents and the longer CNT lengths (the crystallization rate in the stretch-induced polymer melting stage is negative; the lower the value, the faster the crystal melting process). In addition, the crystallization rates in the stretch-induced polymer melting stage in the interfacial regions of the systems filled with more CNTs (the L36-8 system and the L73-4 system) are also lower than those of the systems filled with less CNTs (the L36-4 system and the L73-2 system), further demonstrating that the crystal melting in the interfacial regions is more significant. In short, those above simulation results confirm that the presence of the CNTs has a significant effect on the melting of the crystals around them. The systems with higher CNT contents have higher volume of the interfacial regions, and then more crystals existing in the interfacial regions would melt during stretching; the systems with longer CNTs have stronger ability to induce heterogenous

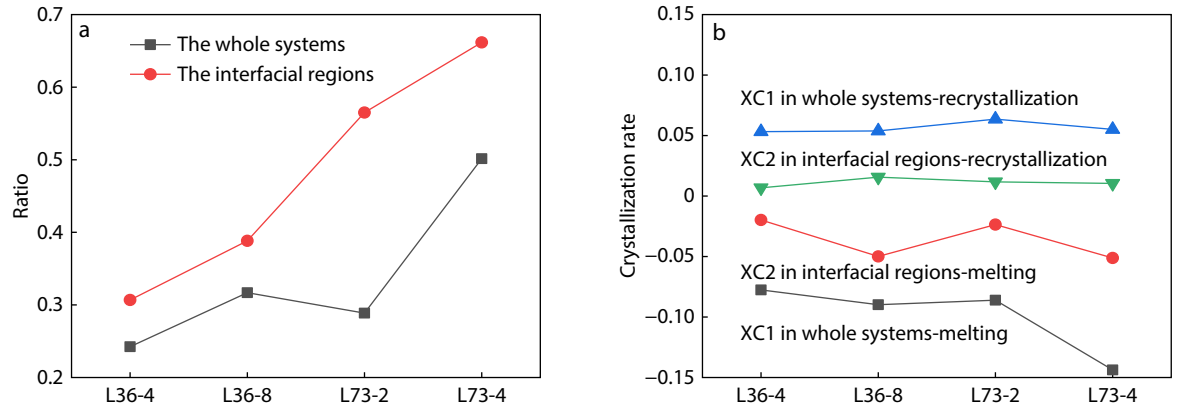

Fig. 8 (a) The ratios of the maximum value of crystallinity decrease in the whole systems/in the interfacial regions to the corresponding initial crystallinity values at the state before stretching (strain = 0) in the four systems; (b) The average crystallization rates at two stretching stages (the stretch-induced crystal melting stage and the stretch-induced polymer recrystallization stage) in the whole systems and in the interfacial regions, respectively.

https://doi.org/10.1007/s10118-023-2974-7

nucleation of chain segments,[10,67] and then more crystals can form in the interfacial regions, which would melt during stretching. In the experimental work of Wang *et al*., they also observed that the crystallinity decreases in the poly(ε-caprolactone)/carbon nanotube nanocomposites are obviously greater than that in the unfilled poly(ε-caprolactone),[69] which is consistent with our current findings.

We further explored how the CNTs affect the stretch-induced melting process of polymer crystals in the interfacial regions. Fig. 9 illustrates the crystalline morphologies in the L36-4 system at different strains. It can be seen that the degree of orientation of the CNT axes and the crystalline stems of PE along the stretching direction increases gradually with the increase of strain. In experiments, it was also found that crystals rotate and orient along the stretching direction during stretching of the crystallized polymers.[18,22,29,69] In addition, during the stretching process the number of the crystalline stems in the interfacial regions decreases first and then increases, indicating that the crystals at the interfacial regions (the red lines in Fig. 9) are prone to melting during stretching. The reason why the crystals in the interfacial regions are more likely to undergo stretch-induced melting may be related to the orientation motions of the CNTs and the polymer chain segments induced by stretching.

Fig. 10(a) shows the changes of the orientational-order parameters of the PE bonds along the stretching direction during stretching in the four systems. It can be seen that the orientational-order parameters of the PE bonds along the stretching direction increase with the increase of strain, demonstrating that stretching can cause the PE bonds in those systems to orient along the stretching direction.[2,15,16,26,32,34–38,41,48,50,53,54,66] In experiments, it was demonstrated that the rotation and the orientation of crystals along the stretching direction occur before the fibrillar texturing (the recrystallization stage) upon tensile drawing.[19,23,70] In simulations, Yamamoto found that stretching can cause the melting and recrystallization of the unoriented crystals in crystallized PE,[58] implying that the stretch-induced crystal melting is closely related to the orientation condition of the corresponding crystals. The values of the critical strain for recrystallization (namely, the minimum values of the crystallinity curves in Fig. 7a) and the values of the saturation strain for segment orientation (corresponding to the turning points of the orientational-order parameter curves in Fig. 10a) are further listed in Fig. 10(b). The turning points of

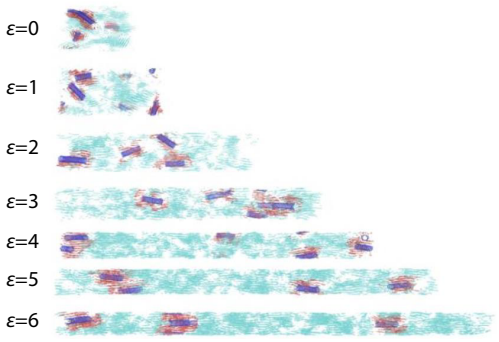

Fig. 9 Snapshots of crystalline morphologies in the L36-4 system at different strains (ε).

the orientational-order parameter curves were defined as the strains corresponding to the intersections of two linear fitting lines in the high strain region and the low strain region (the turning point for the L36-4 system was marked in Fig. 10a). Interestingly, it can be seen that the values of the two different strains are almost the same, except for those in the L73-4 system, demonstrating that the crystal melting during stretching is corelated with the crystal orientation. That is, the stretching can induce the rotation and orientation of crystals along the stretching direction, accompanied by the crystal melting. When chain segments are basically aligned along the stretching direction, further stretching will cause the highly oriented amorphous chain segments to recrystallize into oriented crystals along the stretching direction.[25] That is, when the recrystallization is dominant during stretching, most of the chain segments are highly oriented along the stretching direction. In this condition, the recrystallization rate of highly oriented segments will be independent of the CNT length and content, as shown in Fig. 8(b). The reason for the large difference between the two strain values of the L73-4 system can be attributed to the influence of the CNTs with the high length and content. Fig. 10(c) shows the changes of the orientational-order parameters of the CNT axes along the stretching direction during stretching. Similarly, the orientational-order parameters of the CNT axes increase with the increase of strain, indicating that the CNTs also orient during stretching. To be specific, the orientational-order parameters of the CNT axes in the L36-4 and the L36-8 systems grow faster compared with those in the L73-2 and the L73-4 systems, and the L73-4 system has the slowest growth of the orientational-order parameters, indicating that it is more difficult for the CNTs with high lengths and high contents to orient during stretching. The CNTs with shorter length or lower content can orient easier during stretching, and then the orientation of the corresponding CNTs along the stretching direction can be saturated at lower strain, which is beneficial for the recrystallization of the amorphous chain segments in the interfacial regions at lower strain. In other words, the relatively slow orientation process of the CNTs with long length and high content can make more crystals in the interfacial regions melt, and is also not conducive to recrystallization of the amorphous chain segments in the interfacial regions. Thus, the critical strain for recrystallization in the L73-4 system is highest, as shown in Figs. 7(a) and 10(b). This result further demonstrates that the crystal melting and recrystallization processes are significantly affected by the orientation process of the CNTs. Fig. 10(d) shows the changes of the orientational-order parameters of the PE bonds in the interfacial regions along the corresponding CNT axes during stretching. The orientational-order parameters of the PE bonds in the interfacial regions first decrease and then increase with the increase of strain. In the process of stretching, due to the stretch-induced crystal melting and the orientation motion of the CNTs, the polymer crystals in the interfacial regions are more likely to be damaged, resulting in the decrease of the degree of orientation of the interfacial chain segments along the CNT axes at low strains. With the further progress of stretching, the CNTs and the interfacial chain segments orient gradually along the stretching direction, and in the mean-

https://doi.org/10.1007/s10118-023-2974-7

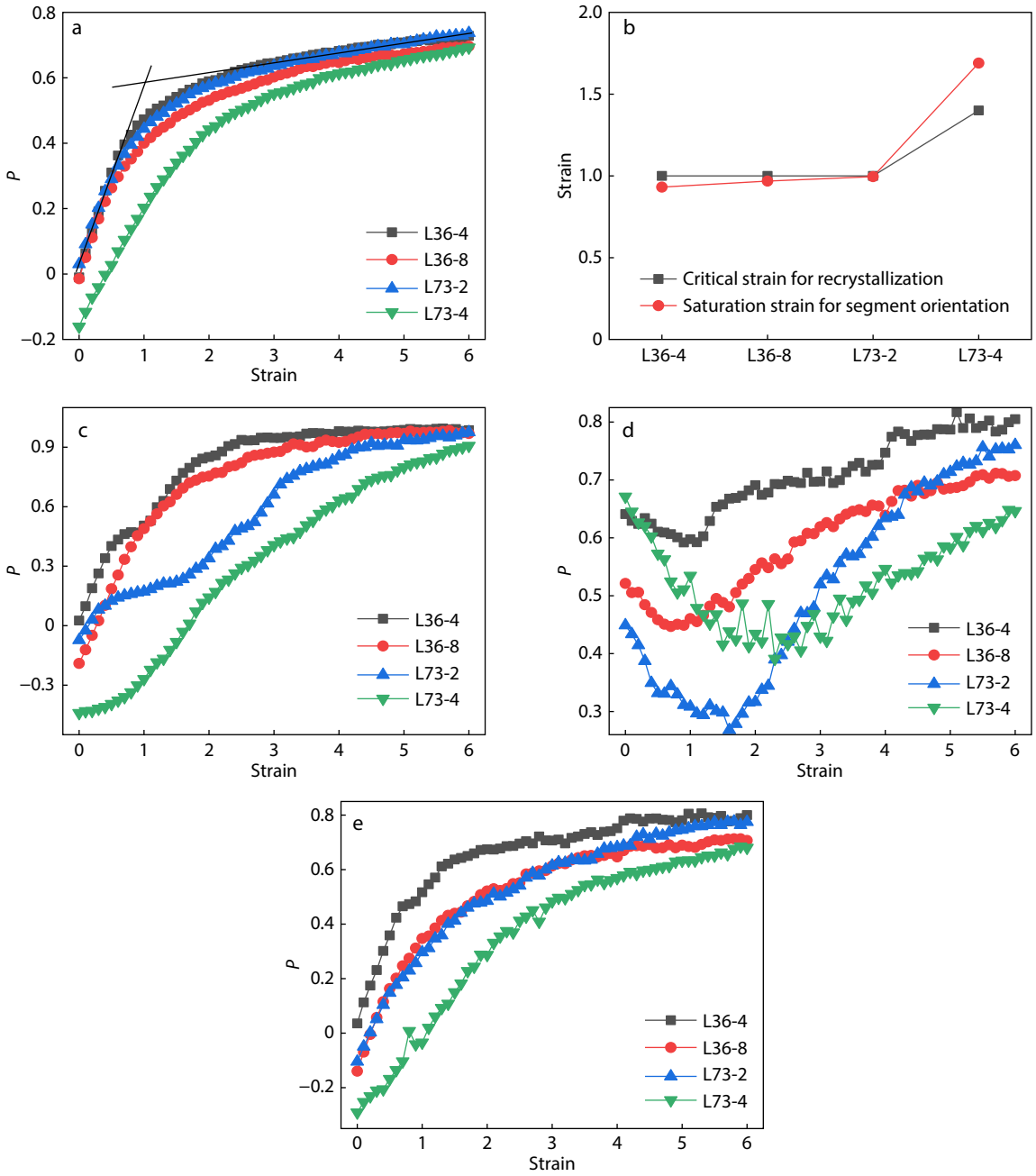

Fig. 10 (a) Changes of orientational-order parameters of PE bonds in the PE/CNT nanocomposite systems along the stretching direction; (b) Critical strain values for recrystallization and saturation strain values for segment orientation; (c) Changes of orientational-order parameters of the CNT axes in the PE/CNT nanocomposite systems along the stretching direction; (d) Changes of orientational-order parameters of PE bonds in the interfacial regions of the PE/CNT nanocomposite systems along the CNT axes; (e) Changes of orientational-order parameters of PE bonds in the interfacial regions of the PE/CNT nanocomposite systems along the stretching direction.

time polymer recrystallization occurs in the interfacial regions, leading to the increase of the degree of orientation of the chain segments in the interfacial regions along the CNT axes at high strains. It should be noted that the orientational-order parameters of the chain segments in the interfacial regions of the L73-2 system and the L73-4 system along the CNT axes decrease more significantly and at faster rates than those of the L36-4 system and the L36-8 system at low strains. Moreover, the values of the strain at which the orientational-order parameters begin to increase (*i.e.*, the minimum values in the curves of the orientational-order parameters) for the systems with the higher CNT lengths (the L73-2 system and the L73-4 system) are higher than those for the systems with the lower CNT lengths (the L36-4 system and the L36-8 system). Combined with the above findings (polymer crystallinity decreases more in the interfacial regions of the systems with the higher CNT lengths or the higher CNT contents, as shown in Fig. 7d), it can be proved that the reason why the

https://doi.org/10.1007/s10118-023-2974-7

orientational-order parameters decrease more in the systems with the longer CNT lengths or the higher CNT contents could be attributed to that the PE crystals in the interfacial regions are more likely to be destroyed or melted. Fig. 10(e) shows the changes of the orientational-order parameters of the PE bonds in the interfacial regions along the stretching direction in the different systems. With the increase of strain, the orientational-order parameters of the PE bonds in the interfacial regions along the stretching direction increase gradually. In addition, the orientational-order parameters of the PE bonds in the interfacial regions of the systems with the longer CNT lengths or the higher CNT contents are lower than those of the systems with the shorter CNT lengths or the lower CNT contents at same strains, indicating that it is more difficult for the interfacial chain segments in the systems with the longer CNT lengths or the higher CNT contents to orient along the stretching direction. In this condition, the interfacial chain segments are more susceptible to the CNTs, and then stretch-induced crystal melting will be more significant in the interfacial regions of the systems with the longer CNT lengths or the higher CNT contents.

In order to more clearly reveal the influence of the CNTs on the orientation of interfacial chain segments, we compared the orientational-order parameters of the PE bonds in the interfacial regions and in the non-interfacial regions along the stretching direction in the four PE/CNT nanocomposite systems. As shown in Fig. 11, compared with the bonds in the non-interfacial regions, the orientational-order parameters of the bonds in the interfacial regions along the stretching direction are closer to those of the CNT axes, suggesting that the orientation of the PE bonds in the interfacial regions is more susceptible to the orientation motion of the CNTs. Besides, the values of the orientational-order parameters of the bonds in the interfacial regions along the stretching direction and the CNT axes along the stretching direction in the L73-4 system are much lower than those in the other three systems at same strains, suggesting that the slow orientation process of the CNTs in the L73-4 system retards the orientation of the bonds in the interfacial regions. In this condition, the orientational-order parameters of the bonds in the whole L73-4 system would become saturated at higher strains, and then the saturation strain corresponding to the turning point of the orientational-order parameter curve of the all bonds will be higher than the critical strain for recrystallization, as shown in Fig. 10(b). Herein, the CNTs in the L73-4 system have obviously larger size compared with the chain segments with the same length. Then, the CNTs have lower mobility, and are oriented more slowly during stretching.

Some previous experimental work revealed that stretching can cause crystal fragmentation in the crystallized semi-crys-

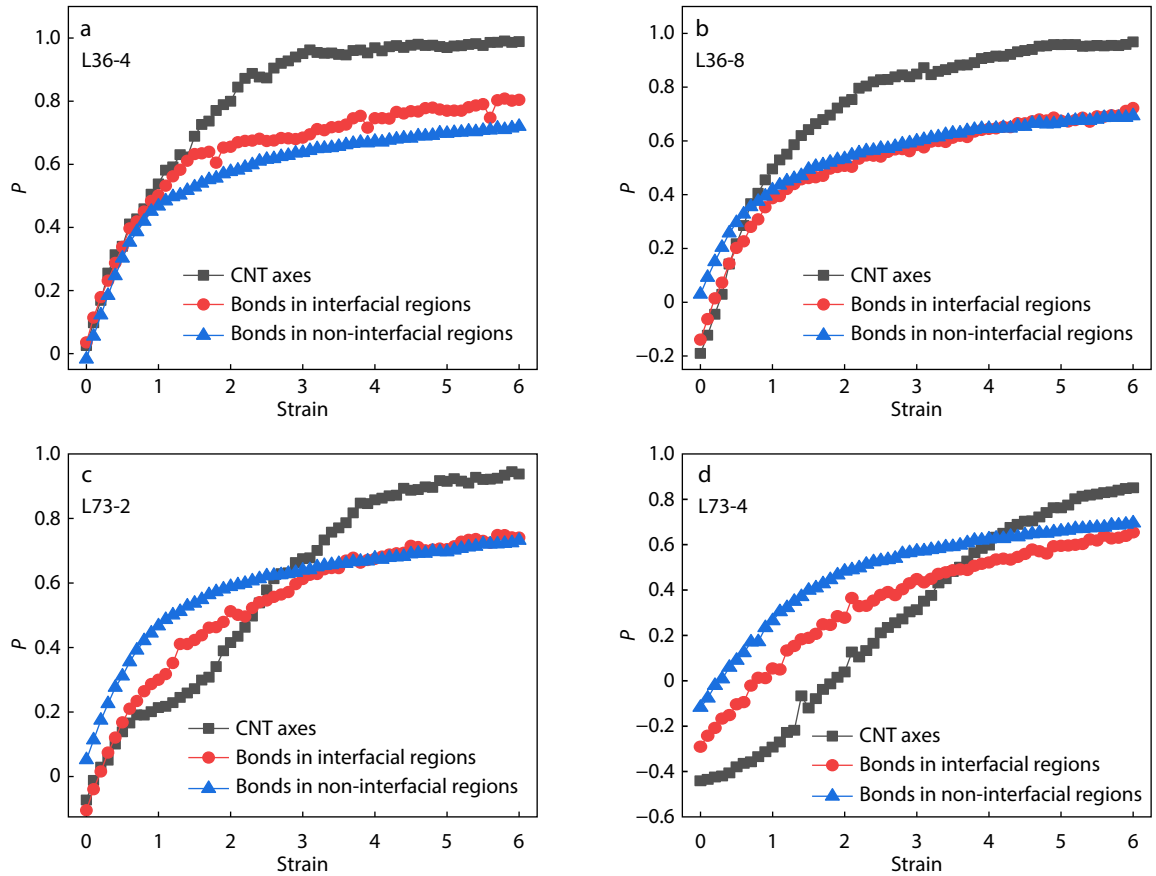

Fig. 11 Changes of the orientational-order parameters of CNT axes along the stretching direction, the orientational-order parameters of PE bonds in the interfacial regions along the stretching direction and the orientational-order parameters of PE bonds in the non-interfacial regions along the stretching direction in the PE/CNT nanocomposite systems: (a) L36-4 system, (b) L36-8 system, (c) L73-2 system and (d) L73-4 system.

https://doi.org/10.1007/s10118-023-2974-7

talline polymers.[18,19,23–25] Thus, we investigated the detailed evolution process of crystal morphology during stretching. Fig. 12 illustrates the crystalline morphologies of the four systems at several strains in the stretch-induced crystal melting stage. In Fig. 12, each region with the same color represents one crystal, and the blue sticks represent the CNTs. In the L36-4 system, it can be seen that the yellow, the purple and the green crystals move during stretching and gradually merge into a larger crystal; the red and the blue crystals gradually disappear. It can be clearly seen that the melting of the crystals around the CNTs is more significant; the surfaces of the CNTs at strain of 0 are surrounded by polymer crystals, and then the CNT surfaces are gradually exposed during stretching due to the crystal melting. In the L36-8 system, the purple and the yellow crystals around the CNTs disappear first during stretching under the influence of the CNT motions; the largest green crystal is divided into two crystals due to the stretching and the movement of the CNTs, and then the two crystals gradually melt during stretching but do not completely disappear, one of which further merge with other crystals to form a new crystal during stretching; the orange and the red crystals gradually merge with the broken crystals around them during stretching; the black crystal existing in the moving path of the CNTs gradually melts under the influence of the CNT motion. In addition, the simulation results of the two systems (the L36-4 system and the L36-8 system) indicate that the small crystals are more likely to melt and disappear, while the large crystals are more stable[71,72] and may survive in the stretching process, but are more likely to break into smaller crystals. Thus, it is difficult for the larger crystals to melt completely during stretching, and they will have a higher chance of merging with other crystals to form new ones. In the systems with the higher CNT contents, on one hand, the size of the crystals is small and the corresponding stability is relatively poor; on the other hand, the stretch-induced movement of the CNTs will also have a negative impact on the crystal stability. Thus, the crystals in the systems with the higher CNT contents are more prone to fragmentation and melting. In the L73-2 system, during stretching, the purple and the blue crystals simultaneously decrease in size and move, and finally merge into a new crystal; the green crystal around the CNTs melts first and finally disappears in the stretching process. In the L73-4 system before stretching, all the CNTs exhibit similar orientations (the CNT axes are perpendicular to the stretching direction), and then the polymer crystals induced by the different CNTs are all connected to form a large crystal (the blue crystal); with the increase of strain, the large crystal splits into different crystals, the size of which gradually decreases, and it takes larger strains for the corresponding crystals to melt or disappear, compared with the other systems (namely, the critical strain for recrystallization is higher). In short, in the systems containing longer CNTs or more CNTs, the stretch-induced crystal melting and fragmentation will be more pronounced due to the orientation movement of the CNTs.

In order to reveal the change process of the crystals during stretching more clearly, we tracked the evolutions of each crystal in the four systems under the action of stretching. Fig. 13 shows the crystallinity changes of each crystal in the four systems during stretching. The dashed lines in Fig. 13 represent the connections between the corresponding crystals (*i.e.*, crystals are broken into some small crystals or some crystals merge into a large crystal), and the colors of the curves are the same as those of the crystals in Fig. 12. It can be seen in Fig. 13(a) that the crystallinity of the yellow and the purple crystals in the L36-4 system gradually increases with the increase of strain, while that of the other three crystals gradually decreases. Based on the crystalline morphology changes in Fig. 12, it can be further confirmed that the yellow and the purple crystals gradually move close to each other to form a big crystal during stretching (this also demonstrates that the crystals can move as a whole during stretching), which then grow during stretching, resulting in the increase of crystallinity. It should be noted that some crystals can grow even at the stretch-induced crystal melting stage (but the crystal melting dominates in this stage).[29] As shown in Fig. 13(b), in the L36-

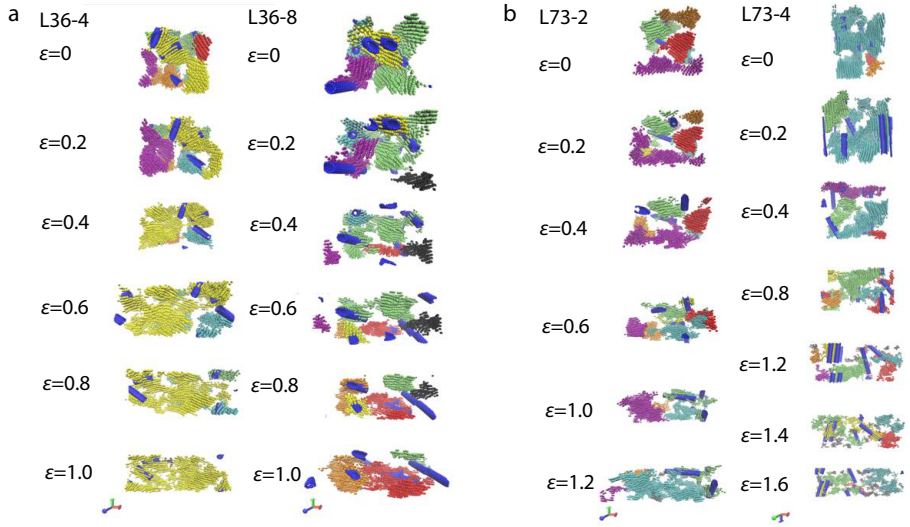

Fig. 12 Snapshots of crystalline morphologies of the PE/CNT nanocomposite systems: (a) L36-4 and L36-8 systems and (b) L73-2 and L73-4 systems at several strains in the stretch-induced crystal melting stage.

https://doi.org/10.1007/s10118-023-2974-7

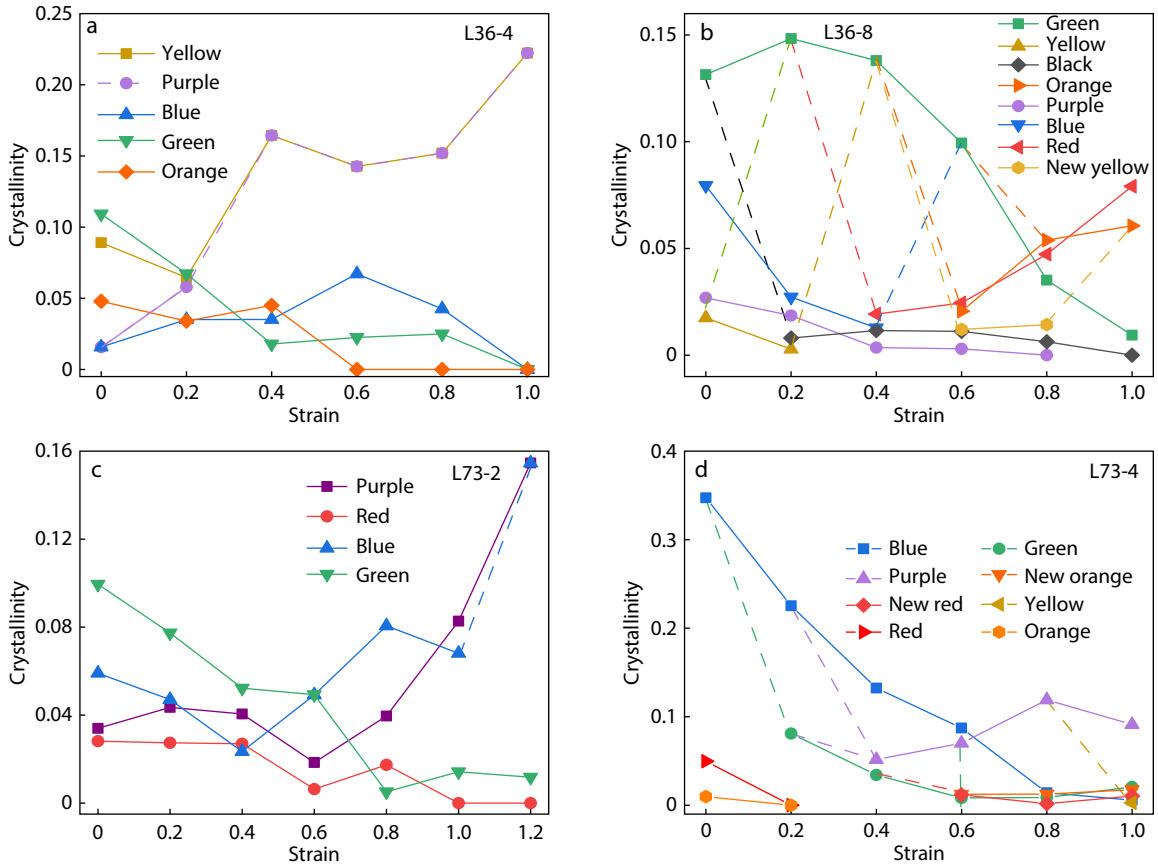

Fig. 13 Evolution of the crystallinity of each crystal with strain in different systems: (a) L36-4 system, (b) L36-8 system, (c) L73-2 system and (d) L73-4 system during stretching.

8 system, the crystallinity of the yellow crystal, the purple crystal and the blue crystal decrease with the increase of strain, indicating that those three crystals melt gradually during stretching; the yellow crystal gradually merges into the green crystal, and the blue crystal merges with the green crystal at the strain of 0.6. The changes of those crystals are mainly affected by the orientation of the CNTs and the movement of the crystals themselves caused by stretching. The largest green crystal gradually splits into the black crystal, the red crystal, the orange crystal and another yellow crystal at different strains during stretching. With the further increase of strain, the crystallinity of the black crystal with small size decreases and becomes 0 at the strain of 1.0 (the black crystal finally disappears), while that of the red crystal and the orange crystal increases (those two crystals grow during stretching). In short, in the stretch-induced crystal melting stage, stretching can cause the fragmentation of big crystals and the melting of small crystals. In the meantime, during stretching, some crystals with relatively large size could grow up, while those with relatively small size could melt and finally disappear. In the L73-2 system, it can be seen that the crystallinity of the purple and the blue crystals decreases first and then increases during stretching, while that of the red and the green crystals gradually decreases. Based on the crystalline morphology changes in Fig. 12, it can be seen that the purple crystal melts and fractures during stretching, and then merges with the blue crystal to form a new crystal. The green crystal is located near the CNTs, and then melts to become smaller due to the orientation movement of the CNTs. In the L73-4 system, it can be seen that the red and the orange crystals existing in the state at the strain of 0 melt and disappear in the stretching process. The largest blue crystal connecting the different CNTs gradually breaks into the green crystal and the purple crystal under the effect of the orientation movement of the CNTs. With the further increase of strain, more new crystals (the yellow, the red and the orange crystals) split from the green and the purple crystals.

It should be noted that graphene sheets belong to an anisotropic two-dimensional filler, which will be also oriented along the stretching direction during stretching. Thus, the crystals in interfacial regions will also melt or break due to the orientation motions of graphene sheets. However, graphene sheets and CNTs have different shapes, may resulting in different orientation ability during stretching, then affecting the melting or fragmentation of crystals. Thus, we plan to investigate the effect of graphene on crystal melting and fragmentation in the future. Besides, there are two other cases to consider. Firstly, the interactions between polymers and nanofillers may also influence the stretch-induced crystal melting and fragmentation. For instance, in the system containing polymer chains grafted onto the CNT surfaces, the interfacial interactions between the polymer chains and the CNTs will be improved. In this condition, the crystals in the interfacial regions should be more stable. Secondly, since the orientation

https://doi.org/10.1007/s10118-023-2974-7

motion of the CNTs could affect the stretch-induced crystal melting or fragmentation, the initial orientation of CNT may also affect the crystal melting or fragmentation during stretching. That is, the interfacial crystals in the systems containing the CNTs with orientation perpendicular to the stretching direction should be easier to melt or break compared with those in the systems containing the CNTs with orientation parallel to the stretching direction.

In short, there are three main phenomena in the stretching process of crystallized polymers: crystal melting, crystal fragmentation and crystal merging. During stretching, small crystals are more likely to melt and disappear, while large crystals are more likely to split into smaller crystals. Crystals that are close to each other will merge during stretching to form a new crystal. In addition, the orientation movement of the CNTs will make the crystals near them easier to melt and break. Our simulation findings demonstrate that both crystal fragmentation and melting occur at low strains during stretching, which is different from the two former different deformation mechanisms (the crystal slip and fragmentation model[19,23,24] and the stress-induced melting and recrystallization model[20,37]). Previously, Men proposed the model of interpenetrated networks to explain the tensile deformation mechanism in semi-crystalline polymers, which unifies the crystal slip and fragmentation model and the stress-induced melting and recrystallization model, occurring at small and large strain regimes, respectively.[25] There are some differences between the interpenetrated network model and our current simulation results. Our above findings show that the crystal melting occurs in the low strain regime rather than the high strain regime. As mentioned above, the occurrence of stretch-induced crystal melting depends on the crystal size and the orientation motion of the CNTs. In the current simulations, the crystals with small size and those near the CNTs melt during stretching. However, if semi-crystalline polymers contain relatively large and perfect crystals corresponding to the global hard crystalline skeleton in the Men's model, crystal slip and fragmentation would occur first.[25] In other words, our simulation results do not contradict the Men's model, but complement it.

The reinforcement mechanisms in polymer nanocomposites could be explained based on the current simulation findings. In the current simulations, it was found that the crystals in interfacial regions of the systems with more CNTs or longer CNTs are easier to melt or break during stretching. This means that more energy input is required to induce the corresponding crystals to melt or break in the systems with more CNTs or longer CNTs, which will then exhibit higher stress during stretching. That is, the systems with more CNTs or longer CNTs will have better mechanical strength.

CONCLUSIONS

In this work, MD simulations were used to investigate the stretch-induced structural changes in the crystallized PE/CNT nanocomposites. During the quiescent crystallization, the CNTs can induce the heterogenous nucleation of chain segments in the interfacial regions. There are more crystals in the interfacial regions of the PE/CNT nanocomposite systems with higher CNT contents. During stretching, polymer crystallinity decreases first and then increases with the increase of strain, indicating that stretching can cause crystal melting and recrystallization. The crystals in the interfacial regions are easier to melt compared with those away from the CNTs due to the effect of the orientation motion of the CNTs induced by stretching. In the systems containing longer CNTs or more CNTs, more polymer crystals would be susceptible to the effects of the CNT movement, causing more crystals to melt. In the stretch-induced crystal melting stage, crystal size is an important factor affecting the crystal changes. Large crystals would be stretched to split into several smaller crystals, while small crystals would be stretched to melt and disappear. In addition, some crystals that are close to each other will merge to form a new crystal. When the orientation of chain segments is saturated along the stretching direction, the recrystallization of highly oriented chain segment dominates the structure changes with the further increase of strain.

Conflict of Interests

The authors declare no interest conflict.

Electronic Supplementary Information

Electronic supplementary information (ESI) is available free of charge in the online version of this article at http://doi.org/10.1007/s10118-023-2974-7.

ACKNOWLEDGMENTS

This work was financially supported by the National Natural Science Foundation of China (No. 52173020).

REFERENCES

1 Ning, N. Y.; Fu, S. R.; Zhang, W.; Chen, F.; Wang, K.; Deng, H.; Zhang, Q.; Fu, Q. Realizing the enhancement of interfacial interaction in semicrystalline polymer/filler composites *via* interfacial crystallization. *Prog. Polym. Sci.* **2012**, *37*, 1425–1455.
2 Nie, Y. J.; Huang, G. S.; Qu, L. L.; Wang, X. A.; Weng, G. S.; Wu, J. R. New insights into thermodynamic description of strain-induced crystallization of peroxide cross-linked natural rubber filled with clay by tube model. *Polymer* **2011**, *52*, 3234–3242.
3 Yang, J. H.; Wang, C. Y.; Wang, K.; Zhang, Q.; Chen, F.; Du, R. N.; Fu, Q. Direct formation of nanohybrid shish-kebab in the injection molded bar of polyethylene/multiwalled carbon nanotubes composite. *Macromolecules* **2009**, *42*, 7016–7023.
4 Xu, J. Z.; Zhong, G. J.; Hsiao, B. S.; Fu, Q.; Li, Z. M. Low-dimensional carbonaceous nanofiller induced polymer crystallization. *Prog. Polym. Sci.* **2014**, *39*, 555–593.
5 Crosby, A. J.; Lee, J. Y. Polymer nanocomposites: the "nano" effect on mechanical properties. *Polym. Rev.* **2007**, *47*, 217–229.
6 Li, L. Y.; Li, C. Y.; Ni, C. Y. Polymer crystallization-driven, periodic patterning on carbon nanotubes. *J. Am. Chem. Soc.* **2006**, *128*, 1692–1699.
7 Li, L. Y.; Li, B.; Hood, M. A.; Li, C. Y. Carbon nanotube induced polymer crystallization: the formation of nanohybrid shish-kebabs. *Polymer* **2009**, *50*, 953–965.
8 Nie, Y. J.; Zhang, R. J.; Zheng, K. S.; Zhou, Z. P. Nucleation details of nanohybrid shish-kebabs in polymer solutions studied by

molecular simulations. *Polymer* **2015**, *76*, 1–7.
9 Nie, Y. J.; Hao, T. F.; Gu, Z. Z.; Wang, Y.; Liu, Y.; Zhang, D.; Wei, Y.; Li, S. J.; Zhou, Z. P. Relaxation and crystallization of oriented polymer melts with anisotropic filler networks. *J. Phys. Chem. B* **2017**, *121*, 1426–1437.
10 Gu, Z. Z.; Yang, R.; Yang, J.; Qiu, X. Y.; Liu, R. J.; Liu, Y.; Zhou, Z. P.; Nie, Y. J. Dynamic Monte Carlo simulations of effects of nanoparticle on polymer crystallization in polymer solutions. *Comput. Mater. Sci.* **2018**, *147*, 217–226.
11 Liu, R. J.; Yang, L. Y.; Qiu, X. Y.; Wu, H. T.; Zhang, Y. Q.; Liu, Y.; Zhou, Z. P.; Ming, Y. Q.; Hao, T. F.; Nie, Y. J. One-dimensional nanofiller induced crystallization in random copolymers studied by dynamic Monte Carlo simulations. *Mol. Simulat.* **2020**, *46*, 669–677.
12 Liu, R. J.; Zhou, Z. P.; Liu, Y.; Liang, Z. P.; Ming, Y. Q.; Hao, T. F.; Nie, Y. J. Epitaxial orientation and localized microphase separation prior to formation of nanohybrid shish-kebabs induced by one-dimensional nanofiller in miscible diblock copolymers with selective interaction. *Polymer* **2019**, *166*, 72–80.
13 Liu, R. J.; Zhou, Z. P.; Liu, Y.; Liang, Z. P.; Ming, Y. Q.; Hao, T. F.; Nie, Y. J. Differences in crystallization behaviors between cyclic and linear polymer nanocomposites. *Chinese J. Polym. Sci.* **2020**, *38*, 1034–1044.
14 Alonso, Y.; Martini, R. E.; Iannoni, A.; Terenzi, A.; Kenny, J. M.; Barbosa, S. E. Polyethylene/sepiolite fibers. Influence of drawing and nanofiller content on the crystal morphology and mechanical properties. *Polym. Eng. Sci.* **2015**, *55*, 1096–1103.
15 Yang, J.; Liu, Z. F.; Zhou, Z. P.; Ming, Y. Q.; Li, S. M.; Hao, T. F.; Nie, Y. J. Studying the effects of carbon nanotube contents on stretch-induced crystallization behavior of polyethylene/carbon nanotube nanocomposites using molecular dynamics simulations. *Phys. Chem. Chem. Phys.* **2022**, *24*, 16021–16030.
16 Nie, Y. J.; Yang, J.; Liu, Z. F.; Zhou, Z. P.; Ming, Y. Q.; Hao, T. F. Precursor formation and crystal nucleation in stretched polyethylene/carbon nanotube nanocomposites. *Polymer* **2022**, *239*, 124438.
17 An, M. F.; Xu, H. J.; Lv, Y.; Tian, F.; Gu, Q.; Wang, Z. B. The effect of chitin nanocrystal on the structural transition of shish-kebab to fibrillar crystals of ultra-high molecular weight polyethylene/chitin nanocrystal fibers during hot-stretching process. *Eur. Polym. J.* **2017**, *96*, 463–473.
18 Hiss, R.; Lynn, S. H.; Strobl, C. G. Network stretching, slip processes, and fragmentation of crystallites during uniaxial drawing of polyethylene and related copolymers. A comparative study. *Macromolecules* **1999**, *32*, 4390–4403.
19 Bowden, P. B.; Young, R. J. Deformation mechanisms in crystalline polymers. *J. Mater. Sci.* **1974**, *9*, 2034–2051.
20 Flory, P. J.; Yoon, D. Y. Molecular morphology in semicrystalline polymers. *Nature* **1978**, *272*, 226–229.
21 Men, Y. F.; Rieger, J.; Strobl, G. Role of the entangled amorphous network in tensile deformation of semicrystalline polymers. *Phys. Rev. Lett.* **2003**, *91*, 095502.
22 Pawlak, A.; Galeski, A.; Rozanski, A. Cavitation during deformation of semicrystalline polymers. *Prog. Polym. Sci.* **2014**, *39*, 921–958.
23 Séguéla, R. Plasticity of semi-crystalline polymers: crystal slip versus melting-recrystallization. *e-Polymers* **2007**, *7*, 382–391.
24 Peterlin, A. Molecular model of drawing polyethylene and polypropylene. *J. Mater. Sci.* **1971**, *6*, 490–508.
25 Men, Y. F. Critical strains determine the tensile deformation mechanism in semicrystalline polymers. *Macromolecules* **2020**, *53*, 9155–9157.
26 Hu, W. B. Polymer features in crystallization. *Chinese J. Polym. Sci.* **2022**, *40*, 545–555.
27 Hu, W. B. The physics of polymer chain-folding. *Phys. Rep.* **2018**, *747*, 1–50.
28 Lv, F.; Chen, X. W.; Wan, C. X.; Su, F. M.; Ji, Y. X.; Lin, Y. F.; Li, X. Y.; Li, L. B. Deformation of ultrahigh molecular weight polyethylene precursor fiber: crystal slip with or without melting. *Macromolecules* **2017**, *50*, 6385–6395.
29 Wang, Z.; Liu, Y. P.; Liu, C. T.; Yang, J. S.; Li, L. B. Understanding structure-mechanics relationship of high density polyethylene based on stress induced lattice distortion. *Polymer* **2019**, *160*, 170–180.
30 Schrauwen, B. A. G.; Janssen, R. P. M.; Govaert, L. E.; Meijer, H. E. H. Intrinsic deformation behavior of semicrystalline polymers. *Macromolecules* **2004**, *37*, 6069–6078.
31 Lu, Y.; Men, Y. F. Initiation, development and stabilization of cavities during tensile deformation of semicrystalline polymers. *Chinese J. Polym. Sci.* **2018**, *36*, 1195–1199.
32 Liao, T.; Zhao, X. T.; Yang, X.; Coates, P.; Whiteside, B.; Barker, D.; Thompson, G.; Lai, Y. Q.; Jiang, Z. Y.; Men, Y. F. *In situ* synchrotron small angle X-ray scattering investigation of structural formation of polyethylene upon micro-injection molding. *Polymer* **2021**, *215*, 123390.
33 Li, L. B. Chain flexibility and connectivity: the uniqueness of polymer crystallization. *Chinese J. Polym. Sci.* **2023**, *41*, 7–13.
34 Nie, C.; Peng, F.; Cao, R. K.; Cui, K. P.; Sheng, J. F.; Chen, W.; Li, L. B. Recent progress in flow-induced polymer crystallization. *J. Polym. Sci.* **2022**, *60*, 3149–3175.
35 Cui, K. P.; Ma, Z.; Tian, N.; Su, F. M.; Liu, D.; Li, L. B. Multiscale and multistep ordering of flow-induced nucleation of polymers. *Chem. Rev.* **2018**, *118*, 1840–1886.
36 Nie, Y. J.; Gao, H. H.; Yu, M. H.; Hu, Z. M.; Reiter, G.; Hu, W. B. Competition of crystal nucleation to fabricate the oriented semi-crystalline polymers. *Polymer* **2013**, *54*, 3402–3407.
37 Nie, Y. J.; Gao, H. H.; Hu, W. B. Variable trends of chain-folding in separate stages of strain-induced crystallization of bulk polymers. *Polymer* **2014**, *55*, 1267–1272.
38 Nie, Y. J.; Zhao, Y. F.; Matsuba, G.; Hu, W. B. Shish-kebab crystallites initiated by shear fracture in bulk polymers. *Macromolecules* **2018**, *51*, 480–487.
39 Zhu, Q.; Zhou, Z. P.; Hao, T. F.; Nie, Y. J. Significantly improved stereocomplexation ability in cyclic block copolymers. *Chinese J. Polym. Sci.* **2023**, *41*, 432–441.
40 Xu, Y.; Yang, J.; Liu, Z. F.; Zhou, Z. P.; Liang, Z. P.; Hao, T. F.; Nie, Y. J. Stereocomplex crystallization in asymmetric diblock copolymers studied by dynamic Monte Carlo simulations. *Chinese J. Polym. Sci.* **2021**, *39*, 632–639.
41 Liu, R. J.; Nie, Y. J.; Ming, Y. Q.; Hao, T. F.; Zhou, Z. P. Simulations on polymer nanocomposite crystallization. *Polym. Crystal.* **2021**, *4*, e10214.
42 Ko, M. J.; Waheed, N.; Lavine, M. S.; Rutledge, G. C. Characterization of polyethylene crystallization from an oriented melt by molecular dynamics simulation. *J. Chem. Phys.* **2004**, *121*, 2823–2832.
43 Graham, R. S. Understanding flow-induced crystallization in polymers: a perspective on the role of molecular simulations. *J. Rheol.* **2019**, *63*, 203–214.
44 Xiao, H. Y.; Luo, C. F.; Yan, D. D.; Sommer, J. U. Molecular dynamics simulation of crystallization cyclic polymer melts as compared to their linear counterparts. *Macromolecules* **2017**, *50*, 9796–9806.
45 Ma, R.; Xu, D.; Luo, C. F., Effect of crystallization and entropy contribution upon the mechanical response of polymer nano-fibers: a steered molecular dynamics study. *Chinese J. Polym. Sci.* **2023**, *41*, 465-474.
46 Lavine, M. S.; Waheed, N.; Rutledge, G. C. Molecular dynamics simulation of orientation and crystallization of polyethylene during uniaxial extension. *Polymer* **2003**, *44*, 1771–1779.
47 Yang, J. S.; Tang, X. L.; Wang, Z.; Xu, T. Y.; Tian, F. C.; Ji, Y. X.; Li, L. B.

https://doi.org/10.1007/s10118-023-2974-7

Coupling between intra- and inter-chain orderings in flow-induced crystallization of polyethylene: a non-equilibrium molecular dynamics simulation study. *J. Chem. Phys.* **2017**, *146*, 014901.
48 Nie, C.; Peng, F.; Xu, T. Y.; Ding, Y. W.; Sheng, J. F.; Chen, W.; Li, L. B. Biaxial stretch-induced crystallization of polymers: a molecular dynamics simulation study. *Macromolecules* **2021**, *54*, 9794–9803.
49 Yamamoto, T. Molecular dynamics simulation of stretch-induced crystallization in polyethylene: emergence of fiber structure and molecular network. *Macromolecules* **2019**, *52*, 1695–1706.
50 Nie, Y. J.; Gu, Z. Z.; Wei, Y.; Hao, T. F.; Zhou, Z. P., Features of strain-induced crystallization of natural rubber revealed by experiments and simulations. *Polym. J.* **2017**, *49*, 309-317.
51 Zhang, W. L.; Larson, R. G. Direct all-atom molecular dynamics simulations of the effects of short chain branching on polyethylene oligomer crystal nucleation. *Macromolecules* **2018**, *51*, 4762–4769.
52 Iyer, K.; Muthukumar, M. Langevin dynamics simulation of crystallization of ring polymers. *J. Chem. Phys.* **2018**, *148*, 244904.
53 Guo, Y. Q.; Wang, J. P.; Luo, W.; Hu, W. B. Dynamic Monte Carlo simulations of strain-induced crystallization in multiblock copolymers: effects of dilution. *Soft Matter* **2022**, *18*, 3376–3383.
54 Guo, Y. Q.; Luo, W.; Zhang, J.; Hu, W. B. Dynamic Monte Carlo simulations of strain-induced crystallization in multiblock copolymers: effects of microphase separation. *Polymer* **2023**, *264*, 125512.
55 Lee, S.; Rutledge, G. C. Plastic deformation of semicrystalline polyethylene by molecular simulation. *Macromolecules* **2011**, *44*, 3096–3108.
56 Kim, J. M.; Locker, R.; Rutledge, G. C. Plastic deformation of semicrystalline polyethylene under extension, compression, and shear using molecular dynamics simulation. *Macromolecules* **2014**, *47*, 2515–2528.
57 Yeh, I. C.; Andzelm, J. W.; Rutledge, G. C. Mechanical and structural characterization of semicrystalline polyethylene under tensile deformation by molecular dynamics simulations. *Macromolecules* **2015**, *48*, 4228–4239.
58 Yamamoto, T. Molecular dynamics in fiber formation of polyethylene and large deformation of the fiber. *Polymer* **2013**, *54*, 3086–3097.
59 Jabbari-Farouji, S.; Rottler, J.; Lame, O.; Makke, A.; Perez, M.; Barrat, J. L. Plastic deformation mechanisms of semicrystalline and amorphous polymers. *ACS Macro Lett.* **2015**, *4*, 147–150.
60 Jabbari-Farouji, S.; Lame, O.; Perez, M.; Rottler, J.; Barrat, J. L. Role of the intercrystalline tie chains network in the mechanical response of semicrystalline polymers. *Phys. Rev. Lett.* **2017**, *118*, 217802.
61 In't Veld, P. J.; Rutledge, G. C. Temperature-dependent elasticity of a semicrystalline interphase composed of freely rotating chains. *Macromolecules* **2003**, *36*, 7358–7365.
62 Plimpton, S. Fast parallel algorithms for short-range molecular dynamics. *J. Comput. Phys.* **1995**, *117*, 1–19.
63 Paul, W.; Yoon, D. Y.; Smith, G. D. An optimized united atom model for simulations of polymethylene melts. *J. Chem. Phys.* **1995**, *103*, 1702–1709.
64 Brenner, D. W.; Shenderova, O. A.; Harrison, J. A.; Stuart, S. J.; Ni, B.; Sinnott, S. B. A second-generation reactive empirical bond order (REBO) potential energy expression for hydrocarbons. *J. Phys.-Condens. Mat.* **2002**, *14*, 783–802.
65 Marco, C.; Naffakh, M.; Gomez, M. A.; Santoro, G.; Ellis, G. The crystallization of polypropylene in multiwall carbon nanotube-based composites. *Polym. Compos.* **2011**, *32*, 324–333.
66 Liu, Z. F.; Zhou, Z. P.; Ming, Y. Q.; Zhang, S. H.; Hao, T. F.; Nie, Y. J. Molecular dynamics simulations of nucleation details in stretched polyethylene. *Polymer* **2020**, *195*, 122442.
67 Xu, Z. H.; Niu, Y. H.; Wang, Z. G.; Li, H.; Yang, L.; Qiu, J.; Wang, H. Enhanced nucleation rate of polylactide in composites assisted by surface acid oxidized carbon nanotubes of different aspect ratios. *ACS Appl. Mater. Interfaces* **2011**, *3*, 3744–3753.
68 Razavi-Nouri, M.; Ghorbanzadeh-Ahangari, M.; Fereidoon, A.; Jahanshahi, M. Effect of carbon nanotubes content on crystallization kinetics and morphology of polypropylene. *Polym. Test.* **2009**, *28*, 46–52.
69 Duan, T. C.; Li, Y. G.; Song, T.; Yao, G. B.; Jin, J.; Wang, Z. B. Uniaxial tensile deformation of microinjection molded PCL/SWCNTs nanocomposites: effect of interfacial "soft epitaxy" on the structural evolution as studied by synchrotron SAXS and WAXD techniques. *Polymer* **2020**, *198*, 122526.
70 Matsuo, M.; Hirota, K.; Fujita, K.; Kawai, H. Studies on the deformation mechanism of polyethylene spherulites by the orientation distribution function of crystallites. *Macromolecules* **1978**, *11*, 1000–1007.
71 Xu, J.; Heck, B.; Ye, H. M.; Jiang, J.; Tang, Y. R.; Liu, J.; Guo, B. H.; Reiter, R.; Zhou, D. S.; Reiter, G. Stabilization of nuclei of lamellar polymer crystals: insights from a comparison of the hoffman-weeks line with the crystallization line. *Macromolecules* **2016**, *49*, 2206–2215.
72 Reiter, G. Some unique features of polymer crystallisation. *Chem. Soc. Rev.* **2014**, *43*, 2055–2065.

https://doi.org/10.1007/s10118-023-2974-7